Bulg. J. Phys. **39** (2012) 72–91

Electric-Field Effects in Aqueous Suspensions of Beidellite Clay Detected by Electro-Optical and SAXS Experiments

K. Antonova[1], **I. Dozov**[1,2], **P. Davidson**[2], **E. Paineau**[3], **C. Baravian**[4], **I. Bihannic**[3], **L.J. Michot**[3]

[1]Institute of Solid State Physics, Bulgarian Academy of Sciences, Tzarigradsko Chaussee 72, 1784 Sofia, Bulgaria
[2]Laboratoire de Physique des Solides, UMR 8502 CNRS-Université Paris-Sud, Bât. 510, 91405 Orsay Cedex, France
[3]Laboratoire Environnement et Minéralurgie, Nancy Université CNRS-INPL UMR 7569, BP40, 54501 Vandœuvre Cedex, France
[4]Laboratoire d'Energétique et de Mécanique Théorique et Appliquée, Nancy Université UMR 7563 CNRS-INPL-UHP, 2, Avenue de la Forêt de Haye, BP160 54504 Vandœuvre Cedex, France

Received *28 November 2011*

Abstract. We propose an original cell geometry for electric-field studies in aqueous suspensions of colloidal particles. The Kerr cell, traditionally used for such studies, is replaced here by a thin flat sample, sealed in an optical capillary, with the field applied by external electrodes. This geometry prevents electrochemical degradation, minimizes heating and convection artifacts, and enables a direct microscopic observation of the textures. We study the electric-field effects in the nematic and isotropic phases of aqueous suspensions of beidellite clay particles with high aspect ratio, $D/L \approx 300$. In the nematic phase, the electric birefringence and SAXS experiments demonstrate good alignment, with nematic director orientation perpendicular to the field. In isotropic samples, we observe a strong field-induced birefringence $\Delta n(E)$, saturating at moderate fields to a plateau Δn^{sat}. The field-induced order $S(E)$ is negative and saturates to $S^{sat} = -0.5$, indicating a perfect anti-nematic order of the particles. The strong electric effect is explained by considering the polarization of the counterions around the charged particle. The estimated equivalent conductivity of the particle is orders of magnitude larger than the bulk conductivity of the electrolyte, resulting in a metal-like behavior of the beidellite disks under field.

PACS codes: 61.30.Gd ; 61.30.St ; 64.70.pv

1310–0157

1 Introduction

Colloidal suspensions of strongly anisometric nanoparticles usually present a complex phase diagram as a function of the volume fraction of the particles. Particles with high aspect ratio often present anisotropic fluid phases, with long-range orientational order, mainly due to Onsager's steric exclusion mechanism [1]. The symmetry of these lyotropic liquid-crystal phases, such as the nematic phase, is similar to that of thermotropic liquid crystals, comprised of small molecules. However, due to the different forces driving the phase transitions and the larger size of the constituents, the macroscopic properties of the nanoparticle suspensions are quite different from those of thermotropic liquid crystals.

Like other anisotropic fluids, these colloidal suspensions are sensitive to applied magnetic and/or electric fields. Under field, the strongly anisotropic particle is oriented, usually with its symmetry axis either parallel or perpendicular to the field. In the isotropic phase this results in a field-induced nematic-like orientational order, with respectively positive or negative order parameter. In the nematic phase, the particles reorientation is a collective process: the nematic order parameter is only slightly enhanced, but the nematic director rotates, resulting in a well aligned texture of the sample. The field-induced order and alignment of nanoparticle suspensions is an important tool for the characterization of the nanoparticles. In the electric-field case, that is easier to apply in practical devices, one can expect technological applications, similar to the widely spread electro-optical applications of the thermotropic liquid crystals.

Mineral nanoparticles of natural or synthetic origin and their colloidal suspensions have attracted much interest in the last decade. Swelling clay minerals are naturally occurring charged aluminosilicates. They can be fully delaminated in aqueous suspensions at low ionic strength, to give mineral single sheeds with very high aspect ratio, and one may expect anisotropic fluid states for their colloidal suspensions. The existence of an isotropic/nematic (I/N) phase transition for clay colloids has been debated for decades since Langmuir's seminal paper [2]. Recently, three different natural clay minerals (two nontronites and one beidellite) have been shown to exhibit an unequivocal I/N transition at low ionic strength [3–5]. The true mineral liquid crystals [6, 7] obtained in this way can be studied by the classical techniques used for other liquid crystals. The present study is focused on beidellite, a tetrahedrally charged swelling clay mineral with Aluminum in the octahedral layer. It presents a rich phase diagram: upon increasing concentration, an isotropic phase, a biphasic region and a nematic liquid phase are observed before a sol/gel transition takes place [5]. Due to the high aspect ratio, the beidellite particles exhibit a strong anisotropy of electric susceptibility. Under moderately strong electric fields, one then obtains large aligned domains in the nematic phase and strong field-induced orientational order in the isotropic phase of the suspension.

The electric birefringence is a classical method [8–10] to study the field-induced orientation of anisotropic fluids. In the usual Kerr cell, two flat electrodes are immersed directly in the liquid, providing a uniform electric field in the sample. The Kerr cell provides high sensitivity, enabling to study very low volume fractions ($\phi \sim 10^{-5}$). However, the direct contact between the electrodes and the electrolyte results in strong parasitic phenomena influencing the measurement and fast sample degradation, especially in aqueous suspensions.

To minimize the parasitic effects, we propose an original cell geometry, very convenient for electro-optical and X-ray scattering experiments under *in-situ* applied electric field. The suspension is contained in a thin flame-sealed capillary and the field is applied by external electrodes. We demonstrate the advantages of this novel cell geometry in aqueous suspensions of beidellite clay particles. In the nematic phase, we observe fast and efficient reorientation of the director perpendicular to the applied field. In the isotropic phase, we show that the induced nematic order parameter is negative and extremely high, similar to that expected for metal particles with the same aspect ratio, immersed in an insulating liquid. We show that the strong field effect is due mainly to the polarization of the ionic atmosphere around the charged beidellite particles.

2 Cell Geometry and Electro-Optic Set-Up

The electric birefringence is a widely used technique [8–11] to study the electric-field-induced orientation of anisotropic fluids, like colloidal suspensions, molecular liquids and macromolecular solutions. In most experiments, a typical Kerr cell [12–15] is used, with two long ($L_e \sim$ 2–10 cm) flat electrodes, a few millimeters apart, immersed directly in the liquid. Up to several kV of d.c. or a.c. voltage is applied to the electrodes, providing a strong uniform electric field in the space between them. The field-induced orientation is detected from the induced birefringence, measured from the phase shift of a probe beam, propagating parallel to the electrodes. The long optical path ($\sim L_e$) of the Kerr cell provides a high sensitivity in terms of the measured birefringence, enabling to study very low volume fractions ($\phi \sim 10^{-5}$) and to work under 'weak' fields (10–100 V/mm) if needed. However, the Kerr cell also presents several drawbacks, especially in the case of aqueous suspensions. The direct contact between the electrodes and the electrolyte results in a strong current in the suspension and parasitic phenomena influencing the measurement. Fast sample degradation is often observed because of the strong polarization of the electrodes, Faradaic reactions and electrolysis. Joule heating and electrokinetic phenomena create convective flows in the sample, leading to flow alignment and spurious birefringence signals. The light scattering and absorption, integrated over the long optical path of the probe beam, are also difficult to separate from the induced birefringence signal. In addition, a number of more trivial experimental difficulties are also to be taken into account. The Kerr cell is bulky (at least several milliliters of

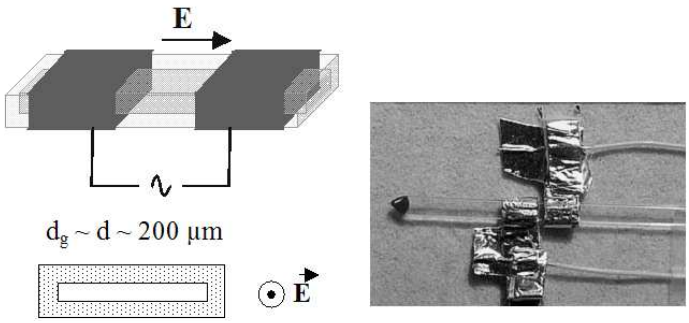

Figure 1. Electro-optic cell in a thin flat optical capillary, with $d = d_g \sim 200\ \mu m$. The field is applied along the capillary axis by using two external electrodes, placed directly on the outside of the capillary glass wall.

suspension are needed for one experiment) and relatively expensive, forbidding long-term storing of the suspension in the cell and periodic repeating of the experiment, *e.g.* to study the time evolution of the system. Direct microscopic observation of the textures during the experiment, which is very important in the case of anisotropic fluids, is difficult with a Kerr cell, due to its specific geometry and large volume. Finally, the sealing of the cell, to protect it from the rapid evaporation of the solvent, is also non-trivial, limiting the lifetime of the sample.

To minimize the parasitic effects and to observe directly the textures of the spontaneous or field-induced liquid-crystal phases, we developed an original experimental set-up [5, 16], inspired by the electro-optical studies in thermotropic liquid crystals [17–21]. The geometry of our sample (Figure 1) is quite different from the usual Kerr cell. The sample container is a thin capillary tube (usually flat optical capillary for the electro-optical experiments and thin-wall (10 μm) cylindrical capillary for the X-ray scattering experiments). The capillary is filled with the suspension and flame-sealed to avoid the evaporation of the electrolyte. To apply the field, we use external electrodes that are made of two rings of metal foil wrapped around the capillary, directly on its outer wall. By applying a high-frequency a.c. voltage to the electrodes, we obtain a strong and uniform electric field in the colloid along the capillary axis. As the electrodes are not physically attached to the walls, their configuration might be varied during the experiment, *e.g.* to select the region of interest for the study.

Our cell geometry presents several advantages compared to the usual Kerr cell. In absence of any direct contact between the electrodes and the suspension, there is no electrochemical degradation of the sample, usually due to electrolysis, charge injection and strong fields in the double electrical layer close to the polarized electrodes. At the high frequency used here, electrokinetic phenomena are too weak to create significant convection and flow alignment of the particles. The Joule heating is still present in our samples but, due to the large

anisotropy of our thin and long cell, the convective flow and the related birefringence are minimized. The probe beam path in our case is very short, a few hundreds of micrometers, minimizing the nuisance when working with strongly scattering (*e.g.* nematic) and/or absorbing systems (*e.g.* dichroic nanoparticles like goethite ones). Moreover, the textures in our sample can be easily observed during the experiment, enabling us to detect any artifact. The microscopic observation is an important advantage in the case of liquid crystalline or biphasic state of the suspension because it allows us to select the region of interest for the study (*e.g.* in polydomain textures) and even to adjust it during the same experiment by moving the capillary within the external electrodes.

Our cell geometry also presents other important advantages from a practical point of view. The sample preparation being easy, fast and very cheap, the cell can be regarded as a disposable item. Because solvent evaporation is prevented by the sealing of the capillary, the cell can be safely stored indefinitely after the study, for additional experiments and investigation of the long-term behavior.

The experimental set-up [16] is presented schematically in Figure 2. The sample is placed on the stage of a Leitz Ortholux polarizing microscope, housing all the optical parts of the set-up (Figure 2). The induced birefringence can be measured directly with the tilting (Berek) compensator C or using the photomultiplier tube PMT. The direct visual measurement with the compensator is insensitive to light scattering and dichroism artifacts. Indeed, the measure does not depend on the absolute transmitted light intensity, but only on the position of the zero-order

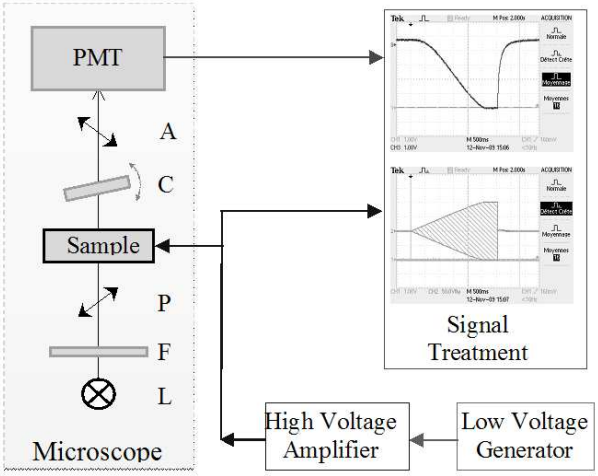

Figure 2. Block scheme of the experimental set-up. The upper oscilloscope trace is the PMT signal, averaged on several pulses and proportional to the phase shift introduced by the sample. The bottom trace is the envelope of the applied a.c. voltage, that linearly increases during the pulse.

interference band minimum. In the more sensitive PMT measurement mode, a phase shift $\delta_c \sim \lambda/4$ is introduced by the compensator and superposed to the optical path difference δ due to the sample birefringence Δn, $\delta = d.\Delta n$. This insures a high sensitivity and a quasi-linear response of the transmitted light intensity $I(\delta)$ for $\delta \ll \lambda/4$:

$$I(\delta) = I_0 \sin^2\left[\frac{\pi}{\lambda}(\delta_c + \delta)\right] \cong \frac{1}{2}I_0 + \frac{\pi}{\lambda}I_0\delta \quad (\text{at } \delta \ll \delta_c = \lambda/4), \quad (1)$$

I_0 being the maximum of the transmitted light intensity, measured at $\delta + \delta_c = \lambda/2$.

The electrical signal applied to the sample is a high-frequency (up to $\nu \sim 1$ MHz) sinusoidal voltage $U = U_0 \cos(2\pi\nu t)$. This signal is either continuous or pulsed, with controlled pulse duration and envelope shape. The generation block synthesizing the low-amplitude signal consists of several function generators and an amplitude modulator.

The signal is amplified in the amplifying block, consisting of a high-voltage amplifier and an optional home-made ferrite-core transformer. Depending on the frequency of the sinusoidal voltage, the maximal amplitude applied to the sample varies from several kilovolts at $\nu < 5$ kHz down to $U_0 = 700$ V at $\nu = 1$ MHz.

The signal from the PMT, proportional to the measured phase-shift (apart from the irrelevant constant $I_0/2$ term that is removed), is amplified and sent to a digital oscilloscope. The high-frequency noise is filtered analogically by the amplifier. The low-frequency noise, that is more difficult to deal with, is numerically filtered by accumulation and averaging of up to 512 bursts on the oscilloscope, preserving the rapid time-response of the system. Finally, the time-dependent signal recorded by the oscilloscope (the upper trace in Figure 2) is proportional to the instantaneous value of the birefringence, induced by the slowly increasing applied field (the bottom trace).

The capillary glass wall, separating the external electrodes from the colloid, seriously affects the field penetration in the sample. Indeed, the field in the cell is defined not only by its geometry (cell thickness d, glass wall thickness d_g and electrode separation distance l), but also by the material properties of the colloid. In a first approximation, the effective r.m.s. value E of the field inside the suspension can be written as

$$E = c_d(\nu)c_s(\nu)\frac{U_0}{\sqrt{2}l}, \quad (2)$$

where the coefficients $c_d(\nu)$ and $c_s(\nu)$ are correction factors for the field attenuation in the sample. They take into account respectively the dielectric mismatch between the glass ($\varepsilon_g \sim 4$) and the electrolyte ($\varepsilon_e \sim 80$) and the screening of the field arising from charge accumulation on the wall/suspension interface.

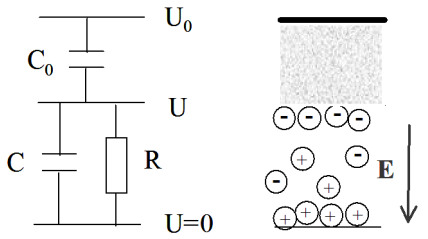

Figure 3. Field penetration in the case of a simple flat sandwich cell geometry. In the equivalent electric circuit C_0 is the capacitance of the two glass walls of the capillary, in series with the capacitance C and the resistance R of the suspension.

Let us estimate the correction factors for the field penetration in the sample for a flat sandwich cell geometry (differing from the actual geometry of our cell by the direction of the electric field) and its equivalent electric circuit (Figure 3). We first consider the field at high frequency $\nu \gg \nu_c$, where $\nu_c = K_e/(2\pi\varepsilon_0\varepsilon_e)$ is the charge relaxation frequency [22] of the suspension, defined by its conductivity K_e and the dielectric constant ε_e of the electrolyte. Then we can neglect R, and the c_d coefficient in Eq. (2) is obtained from the voltage drop across the two glass walls, the capacitance C_0 in the equivalent circuit, in series with the much larger capacitance of the suspension $C = 2C_0(\varepsilon_e d_g)/(\varepsilon_g d)$

$$c_d(\nu) = \frac{U}{U_0} = \frac{C_0}{C + C_0} = \frac{1}{1 + 2\frac{\varepsilon_e d_g}{\varepsilon_g d}} \,. \tag{3}$$

For aqueous suspensions and $d = d_g$ (which is the case of commercial flat glass capillaries) this results in extremely weak penetration of the field in the electrolyte, $c_d(\nu) \approx 1/40 \ll 1$ (however, this geometry remains useful [23] in the case of a moderate dielectric constant of the solvent, or even for aqueous suspensions in the case when the electrodes are in direct contact with the electrolyte [24]).

Due to the finite conductivity of the electrolyte, the voltage U applied to it drives the mobile charges towards the electrodes. The ions are stopped at the interface with the glass wall, building up an electric double layer, decreasing the field in the liquid. At low enough frequency, the ions move in phase with the applied field and the charges accumulate until the field is completely screened in the bulk electrolyte: the screening coefficient becomes $c_s(\nu) \approx 0$ and the effective field in the sample is then negligible. When the frequency ν increases toward ν_c the charge carriers lag behind the field and the screening is only partial. Finally, at $\nu \gg \nu_c$, the charge accumulation during the half-period of the field is negligible and the field penetrates the sample without any screening, $c_s(\nu) \approx 1$. From the equivalent electric circuit in Figure 3, the screening coefficient $c_s(\nu)$ can be calculated analytically

$$c_s(\nu) = \frac{\nu}{\sqrt{\nu^2 + (1 - c_d)^2 \nu_c^2}} \,. \tag{4}$$

We note that the effective relaxation frequency is not ν_c, but $(1 - c_d)\nu_c$, *i.e.*, it depends on the sample geometry through the dielectric attenuation factor $c_d = c_d(\nu)$. In fact, if $c_d \approx 1$, the field penetrates in the sample at frequencies much lower than ν_c, enabling the study of samples with higher conductivities.

The actual geometry of our cell is more complex than the simple flat sandwich cell, making impossible the analytical calculation of the field penetration. However, a rough qualitative analysis can be made by analogy with the previous case. In the area between the electrodes, where the observation takes place, the field lines are now parallel to the glass/liquid interface, instead of perpendicular to it. Then, the glass wall capacitances in this area are in parallel, rather than in series, with the capacitance of the colloidal suspension. (This only holds true around and under the electrodes.) However, for the same wall capacitances, C is now a factor of $d/l \ll 1$ lower than in the sandwich cell case. As a result, we expect a significant increase of the $c_d(\nu)$ factor compared to the sandwich cell case with external electrodes.

Quantitatively, we confirm this conclusion by a numerical calculation of the field in the sample. The results of a finite element analysis at high frequencies ($\nu \gg \nu_c$), using the commercial FlexPDE program, are presented on Figures 4 and

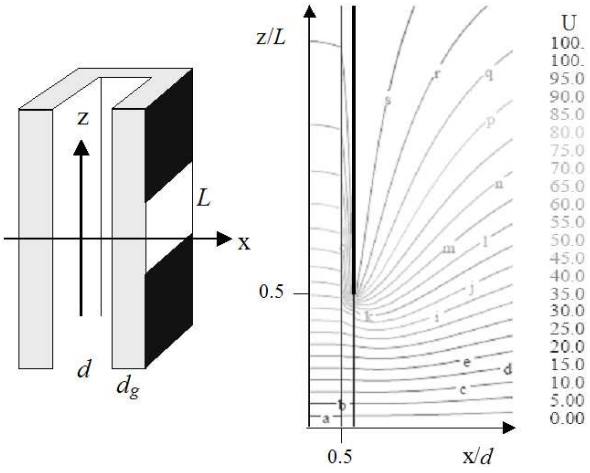

Figure 4. Numerically calculated equipotential surfaces of the electric field in a flat optical capillary. The suspension is in the region defined by $-0.5 < x/d < 0.5$. For simplicity, only the upper-right quadrant is represented, in the cross-section defined by the direction of observation (**x**) and the long axis of the sample (**z**). In the interelectrode area inside the sample, accessible for optical observation, the field **E** is highly uniform and parallel to **z**.

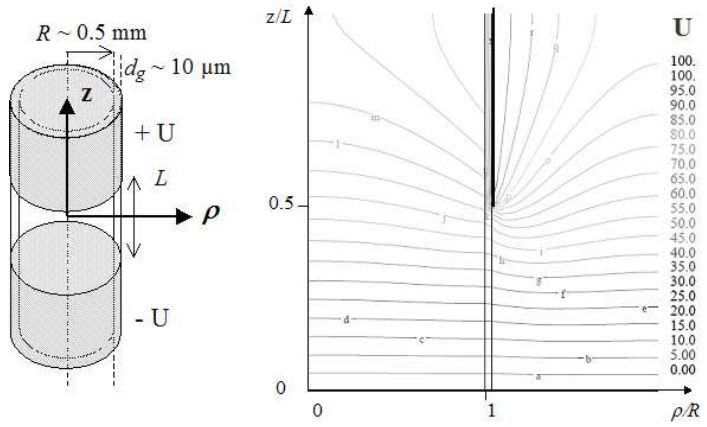

Figure 5. Numerically calculated equipotential surfaces of the field in a cylindrical capillary. The suspension is in the region defined by $\rho/R < 0.5$. Only the upper-right quadrant is represented, in the cross-section defined by the radius (ρ) and the long axis of the capillary (**z**). Inside the sample, the field **E** is again uniform and parallel to **z**.

5, respectively for the cases of a flat optical capillary and a thin-wall cylindrical one. In both cases, in the inter-electrode area of interest, the field in the sample is parallel to the capillary axis and is highly uniform (with a few percent variation close to the electrodes).

For the typical aspect ratios of our samples $l/d \geq 5$, we obtain $c_d(\nu)$ factors in the range of $0.4 - 0.7$, showing a quite effective penetration of the field in the electrolyte. A similar finite element analysis at lower frequencies, $\nu \sim \nu_c$, taking into account the conductivity of the sample, confirms qualitatively the decrease of the relaxation frequency for the field screening by ions upon increasing $c_d(\nu)$ factor. Strictly speaking, in our real geometry, the factorization of the two attenuation coefficients in Eq. (2) is only an approximation but we can use it formally for simplicity. On Figure 6 is presented the screening coefficient calculated numerically, showing again a significant decrease of the critical frequency for the field penetration in the sample for increasing aspect ratio l/d of the cell.

3 Experimental Results

This original cell geometry was used to study the electric-field alignment of aqueous colloidal suspensions of nanoparticles. To demonstrate its advantages for anisotropic colloids, we focus here on some of our results of electro-optic and small angle X-ray scattering (SAXS) studies of the electric-field effects in the isotropic and nematic phases of beidellite clay particles. More detailed studies of the thermodynamic behavior and alignment under external fields have been presented elsewhere [5, 16].

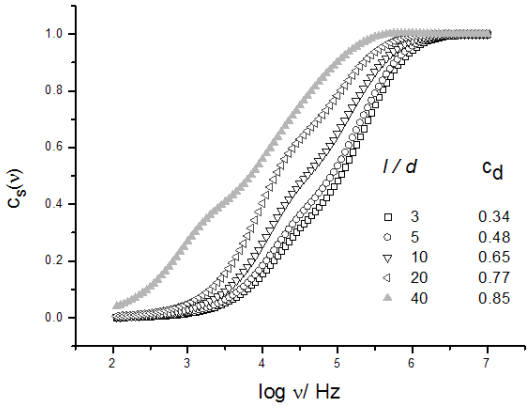

Figure 6. Screening factors numerically calculated for different l/d ratios. The $c_d(\nu)$ factors are shown for $\nu \to \infty$. Realistic values $K_e = 0.003$ S/m and $\varepsilon_e = 80$ are considered, corresponding to a charge relaxation frequency $\nu_c = 690$ kHz. The critical frequency for the field penetration in the sample is significantly lower, ~ 250 kHz for $c_d = 0.34$, and further decreases with increasing aspect ratio l/d.

Beidellite is a natural dioctahedral swelling clay mineral with a charge deficit located in the tetrahedral sheet, resulting from the substitution of Si by Al. Samples of natural beidellite SBId-1 were purified and fractionated following already described procedures [3–5]. The average diameter of "size 2" and "size 3" particles used here was respectively 286 nm and 210 nm [5], the thickness of the individual clay layers being in both cases around 0.65 nm.

Homogeneous suspensions were prepared by osmotic stress and the mass concentrations were determined by weight loss upon drying. Before the electric-field experiments, the capillaries with the beidellite suspensions were stored vertically for a few days, in order to homogenize and relax from flow alignment. For volume fractions $\phi < 4.2 \times 10^{-3}$ the samples are in the isotropic phase. Samples with $4.2 \times 10^{-3} < \phi < 5.9 \times 10^{-3}$ are biphasic. After a few weeks, two well-separated regions are observed in test-tubes and capillaries, isotropic at the top and nematic at the bottom. The measurements were made separately in the isotropic and nematic regions, after phase separation has occurred.

3.1 Nematic Phase under Electric Field

Due to the steric and electrostatic interactions between the highly anisotropic particles, spontaneous long-range orientational order arises in the nematic phase, described by the nematic order parameter tensor $\mathbf{Q}$ [22]

$$Q_{ij} = \frac{3}{2} S_N (n_i n_j - \frac{1}{3}\delta_{ij}). \tag{5}$$

Here $\mathbf{n}$ is the nematic director, a unit vector pointing along the local macroscopic symmetry axis of the phase. The scalar order parameter S_N, typically $S_N > 0.6$ in colloidal nematics, describes the average degree of orientation of the symmetry axis of the particles along the director.

The nematic phase responds strongly to external electric or magnetic fields, with collective reorientation of the particles. The amplitude S_N of the nematic order changes only slightly, the main effect being the reorientation of the director $\mathbf{n}$. Magnetic fields are widely used for the alignment of these colloidal nematics but, apart from particles with strong magnetic properties, *e.g.* goethite [25], very large fields should be applied to obtain well-aligned samples (up to 9 Tesla for beidellite).

Strong electric fields are easier to obtain with less bulky and expensive equipment, making electric-field alignment very convenient for both optical and X-ray scattering experiments. Our original cell geometry further simplifies the electric-field experiment, enabling direct microscopic observation of the nematic textures.

In Figure 7 are presented the typical textures observed in the sample before and after the application of an electric field in the nematic phase of a size 3 beidellite suspension. The photographs are taken using crossed polarizers (indicated by white arrows on the photographs). Before applying the field (Figures 7a and 7b), the texture is inhomogeneous, similar to the nematic schlieren texture, obtained when the director $\mathbf{n}$ is everywhere parallel to the surfaces (*i.e.* lies in the $\mathbf{xz}$ plane in Figure 7e, with $\varphi = 0$), but without well-defined in-plane orientation, *i.e.* with varying angle θ. However, rotating the crossed polarizers, we observe that some regions remain dark, indicating a homeotropic orientation of the director ($\mathbf{n}$ along $\mathbf{y}$, with $\varphi = \pi/2$). More generally, the optical analysis of the texture shows that the sample is completely disoriented, with slow spatial variation of both θ and φ.

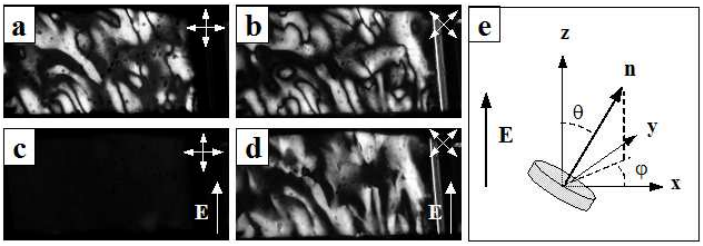

Figure 7. Electric-field alignment of a nematic beidellite suspension (size 3, ionic strength 10^{-4} M, $\phi = 0.56\%$). The field ($\nu = 500$ kHz, $U = 200$ V) is applied in the $z-$direction. The external electrodes, with interelectrode distance $l = 1$ mm, are visible as diffuse shadows on the upper and bottom edges of the photographs.

When a suitable field is applied ($\nu > 200$ kHz, $E > 50$ V/mm), we observe the sample alignment on the time scale of a few minutes (the same effect is obtained after several hours under a 9 T magnetic field). With the field parallel to one of the polarizers (Figure 7c), the field of view becomes uniformly dark, indicating that the director $\mathbf{n}$ is either parallel ($\theta = 0$) or perpendicular ($\theta = \pi/2$) to $\mathbf{E}$. The rotation of the polarizers (Figure 7d) reveals that $\mathbf{n}$ is perpendicular to $\mathbf{E}$, with degenerated φ-orientation. This confirms the expected negative dielectric anisotropy of the flat beidellite discs.

The brighter regions in Figure 7d correspond to $\varphi = 0$ and maximum optical retardation $\delta = d.\Delta n$ of the cell. The best estimate $\Delta n = -4.7 \times 10^{-4}$, obtained from the measured local phase shift in the size 3 beidellite suspension (ionic strength 10^{-4} M, $\phi = 0.62\%$), is in reasonable agreement with the value measured in a magnetic-field aligned sample.

For dilute suspensions, we expect

$$\Delta n_N = \Delta n^p \phi S_N \,, \tag{6}$$

where Δn^p is the specific birefringence of the particles, *i.e.* the value extrapolated to $\phi = 1$ and $S_N = 1$. The negative value measured for Δn confirms the negative sign of Δn^p expected for flat disks. However, the birefringence measurement only gives the product $\Delta n^p S_N$, and we need an additional measurement of one of them, *e.g.* S_N.

For this purpose, we performed SAXS experiments with an already described in-house set-up [26]. The samples were placed in 1 mm cylindrical quartz capillaries and aligned by applying an electric field *in situ*. The SAXS experiment [5], confirms the alignment of the director perpendicular to the field and gives a direct access to the orientational distribution function $f(\theta)$ of the particles, and hence to the order parameter. In Figure 8 is presented $f(\theta)$ obtained from the SAXS pattern of a size 3 beidellite suspension, aligned *in situ* by an electric field. The solid line is a fit with a Maier-Saupe distribution function [27]. After normalization of $f(\theta)$, we obtain the nematic order parameter,

$$S_N = \frac{1}{2}\langle 3\cos^2\theta - 1\rangle = \frac{1}{2}\int_0^1 f(\theta)(3\cos^2\theta - 1)d\cos\theta = 0.80 \pm 0.03. \tag{7}$$

a value slightly higher than that ($S_N = 0.76$) obtained for the same sample aligned under strong magnetic field (applied before the experiment, and not *in situ*). With this measured value of S_N, our best estimate for the specific birefringence of the beidellite particles (needed for the interpretation of the isotropic phase results) is $\Delta n^p = -0.09$.

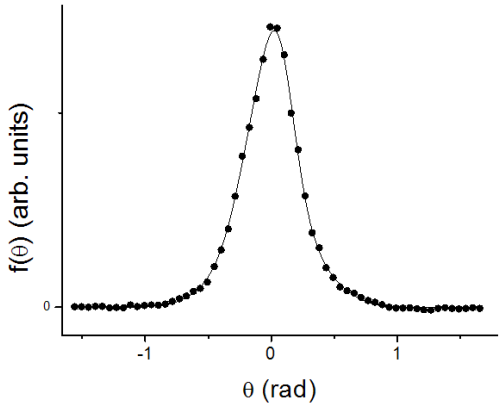

Figure 8. Orientational distribution function measured (points) from the SAXS pattern of a beidellite sample (size 3; ionic strength 10^{-4} M; $\phi = 0.52\%$), aligned by an electric field (40 V/mm, 700 kHz). The fit with a Maier-Saupe distribution (solid line) gives $S_N = 0.80$.

3.2 Isotropic Phase under Electric Field

In dilute solutions, the interactions between the particles are too weak to induce a spontaneous long-range orientational order [25]: the phase is isotropic, with $S_N = 0$. Nevertheless, under strong fields, the individual (uncorrelated) reorientation of the particles results in field-induced order, described again by an order parameter tensor $\mathbf{Q}$(E):

$$Q(E)_{ij} = \frac{3}{2}S(E)(n_i n_j - \frac{1}{3}\delta_{ij}) \tag{8}$$

Here $\mathbf{n}$ is the induced director, given by the average orientation of the particle symmetry axis, the disk normal in our case, and $S(E)$ is the induced order parameter.

Unlike the nematic phase, in the isotropic phase the field torque is applied separately to each particle, resulting in weaker field effects and low values of the induced order parameter. However, for colloidal suspensions of large and strongly anisotropic particles, as beidellite clay sheets, the electric-field effect is orders of magnitude stronger than for molecular liquid crystals. In dilute suspensions, $S(E)$ provides a valuable direct information about the properties of individual nanoparticles, *e.g.* the anisotropy of the particle interaction with the field. For the quantitative interpretation of this information, we need to know the actual field inside the electrolyte. For this purpose, we will systematically refer below to the effective field E r.m.s. value in the suspension, after recalibration with the numerically calculated value of c_d, and with the experimentally measured $c_s(\nu)$ dependence.

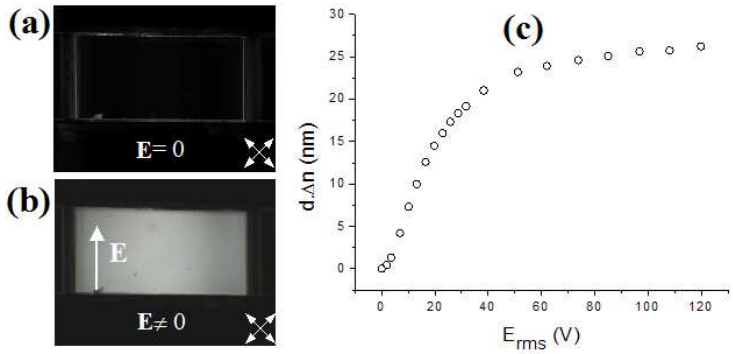

Figure 9. Electric birefringence in the isotropic phase of beidellite clay suspension (size 2; ionic strength 10^{-5} M; $\phi = 0.37\%$). Sample observed between crossed polarizers before (a) and after (b) the application of the field. (c) Phase-shift in the cell ($d = 200$ μm) as a function of the applied effective field in the suspension, $\nu = 700$ kHz.

The typical behavior of the isotropic beidellite suspensions under field is shown in Figure 9. At $E = 0$, the sample is dark between crossed polarizers (Figure 9a). Under field (Figure 9b), the transmission increases, due to the field-induced nematic-like order. The optical anisotropy is uniaxial and positive, with slow axis parallel to the field, along the capillary axis. The typical dependence of the phase-shift $d.\Delta n$, measured as a function of the applied r.m.s. voltage at fixed frequency $\nu = 700$ kHz, is shown in Figure 9c. The usual Kerr regime, with birefringence increasing as E^2, is observed only at very low fields. At $E > 10$ V/mm, the curve deviates from the Kerr regime and rapidly saturates toward a finite $d.\Delta n^{sat}$ value.

Because the birefringence is a function of the internal field in the suspension, it can be very conveniently used as an *internal probe* for the field penetration in the electrolyte. Local measurements of the slow axis orientation and the phase-shift confirm that the field in the sample is parallel to the capillary axis and uniform, as predicted by the finite-element numerical simulation. The curves $\Delta n(U)$, measured at different frequencies, differ only by a scaling factor of the voltage axis, as expected from Eq. (2).

Supposing that $c_s(\nu)$ saturates toward $c_s(\nu) \approx 1$ at high frequency and measuring the voltage $U(\nu)$ needed to obtain a fixed birefringence value, we obtain the screening coefficient $c_s(\nu)$ plotted in Figure 10 for three different experimental geometries, with l/d aspect ratios and c_d factors listed on the figure. The experimental curves follow the general trend predicted by Eq. (4), with better field penetration upon increasing c_d, but the slope of the experimental curves is significantly softer than expected from Eq. (4). The agreement with the numerical simulations is semi-quantitative. The best fit is obtained for $K_e = 6$ mS/m, twice larger than the experimentally measured conductivity $K_e \approx 3$ mS/m (cor-

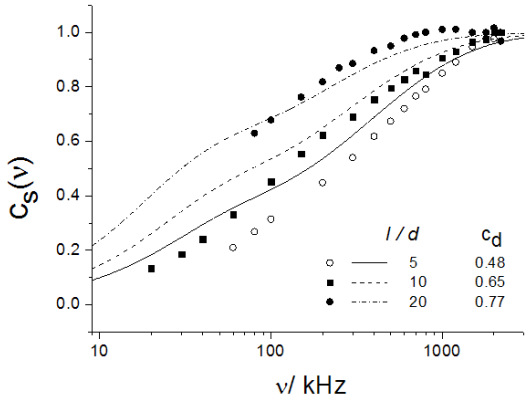

Figure 10. Experimentally measured screening factor (symbols) for three different aspect ratios l/d of the cell, obtained by varying the interelectrode distance l ($d = 200\mu m$, beidellite suspension size 3, ionic strength 10^{-4} M, $\phi = 0.25\%$). The solid lines are the numerical results calculated for the same geometries, assuming bulk conductivity of the electrolyte $K_e = 6$ mS/m.

responding to $\nu_c = 660$ kHz). In all the following experiments, the frequency was fixed at 700 kHz and the experimental value of $c_s(\nu)$ was used for the estimation of the field inside the cell.

For all studied volume fractions, the behavior observed is similar to that in Figure 9c: the Kerr regime remains limited to very weak fields, $E < 30$ V/mm, and saturation to a ϕ-dependent plateau $\Delta n^{sat}(\phi)$ occurs at higher fields. The low value of the saturation field shows a very strong coupling of the beidellite sheets with the field.

Rewriting Eq. (6) for the induced order and using the Δn^p value measured in the nematic phase, we obtain the induced order parameter $S(E)$ as a function of the applied field (Figure 11). For both dilute samples (open symbols) and concentrated ones (measured in the isotropic phase at biphasic coexistence, full symbols), the order parameter is negative. At high fields the order saturates to $S^{sat} = -0.5$, reaching the theoretical limit for a perfect negative orientational order. The induced order is then called "anti-nematic" [25, 28], with director $\mathbf{n}$ parallel to the field and to the beidellite sheets, as shown on the insert of Figure 11. On symmetry grounds [22], the anti-nematic state is not forbidden, but it is never observed in absence of external fields. In fact, the state $S_N < 0$ is not an equilibrium state, but only a saddle point of the nematic free energy [29, 30].

In the same Figure is presented the best fit of the data with $S(E)$, calculated by using a Maier-Saupe distribution function [27, 31]

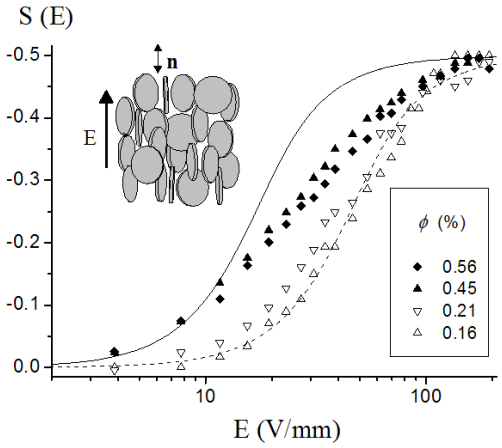

Figure 11. Induced order of the beidellite particles under electric field (size 3, ionic strength 10^{-4} M). The dashed and solid lines are the best fits with $S(E)$ calculated with Maier-Saupe like distribution function, respectively for volume fractions far away and close to the isotropic/nematic phase transition. The insert shows the orientation of the particles at $S(E) \approx -1/2$, the perfect anti-nematic state with director $\mathbf{n} \parallel \mathbf{E}$.

$$f(\theta) = \exp(-U^p(\theta)/kT) / \int_0^1 \exp(-U^p(\theta)/kT) d\cos\theta, \tag{9}$$

where $U^p(\theta)$ is the interaction energy of the particle with the field, quadratic in E in our case:

$$-\frac{U^p(\theta)}{kT} = \text{const} + \frac{1}{2}\Delta A E^2 \cos^2\theta. \tag{10}$$

Here $\Delta A = A_\parallel - A_\perp$ is the anisotropy of the particle excess polarizability, compared to the surrounding medium (and renormalized with kT). The fits on Figure 11 give fairly large values for the coupling coefficients, -2.5×10^{-9} m^{2}V^{-2} and -1.8×10^{-8} m^{2}V^{-2} respectively for the low and high volume fractions data. The additional enhancement by one order of magnitude of ΔA in the latter case is due to the collective reorientation of the particles and the strong interactions between them.

The large negative order parameter induced by the electric field in isotropic beidellite clay suspensions was also confirmed by SAXS experiments. We used again our home-built set-up, applying the electric field to suspensions placed in 1 mm cylindrical quartz capillaries. In Figure 12 is presented a typical SAXS pattern of size 3 beidellite isotropic suspensions, submitted to an electric field *in situ*. Qualitatively, the SAXS experiment confirms the negative (anti-nematic) induced order, with the short axis of the particles aligned perpendicular to the field. More precise SAXS experiments are in progress at the SOLEIL syn-

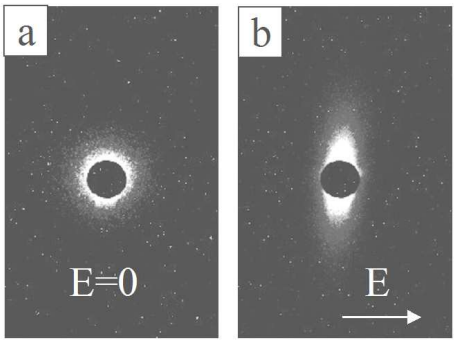

Figure 12. SAXS patterns of the isotropic phase of beidellite colloidal suspension (size 2, ionic strength 10^{-4} M, $\phi = 0.46\%$). (a) Without field. (b) Under electric field ($U = 130$ V r.m.s., $l = 2$ mm, $\nu = 700$ kHz).

chrotron, in France, in order to confirm quantitatively our electro-optic results for *in situ* aligned isotropic beidellite suspensions.

To understand the origin of the very strong coupling of the beidellite particles with the electric field, we need to consider the different physical mechanisms contributing to ΔA. The first one [32] is due to the dielectric contrast between the particle (ε_p) and the surrounding electrolyte (ε_e), resulting in accumulation of bound charges on the interface and in strong induced dipole moment of the particle. Standard electrostatic calculation [33] gives the estimation $\Delta A_d = -\varepsilon_0 \frac{V^p}{kT} \frac{(\varepsilon_p - \varepsilon_e)^2}{\varepsilon_p} \approx -4.6 \times 10^{-11}\ \mathrm{m^2 V^{-2}}$, that is two orders of magnitude lower than the experimentally observed value. So, the dielectric polarization of the particle cannot explain our results, despite the large dielectric contrast $\varepsilon_e/\varepsilon_p \gg 1$ and the extremely strong anisometry $D/L \approx 300 \gg 1$ of the beidellite sheets.

In a similar way, the contrast of the conductivities, K_p and K_e, of the two media leads to accumulation of mobile charges at the interface, *i.e.* to the well-known Maxwell-Wagner (MW) induced dipole moment [34, 35]. At lower frequencies, the MW effect can be very strong, dominating the dielectric term by several orders of magnitude. However, this contribution can be neglected in our experiment because, at the high frequency ($\nu > \nu_c$) used, the mobile charges cannot follow the fast inversions of the applied alternating field.

The third mechanism, involving the polarization of the ionic cloud of the particle, was first pointed out by O'Konski [36, 37] and is important for charged colloids. The resulting Maxwell-Wagner-O'Konski (MWO) induced polarization is often the dominating mechanism for electric field effects [37, 38] in colloidal suspensions. To estimate the MWO contribution we follow the approach proposed by O'Konski [9, 36, 37]. The large concentration of mobile counter-ions in the double layer at the particle/electrolyte interface results in a strong local increase of the conductivity. This additional "surface" conductivity K^σ con-

tributes to the equivalent bulk conductivity of the particle: $K_k^{eq} = K_p + \frac{K_k^\sigma}{\xi_k}$; $k = (\|, \perp)$, where ξ_k is an effective length, depending on the particle shape and dimensions.

Taking advantage from the extremely large D/L ratio of the beidellite disks (D is the average diameter and L the thickness of the beidellite sheet), we obtain [16]

$$K_\perp^{eq} = \frac{2K_\perp^\sigma}{L}; \quad K_\|^{eq} = \frac{4K_\|^\sigma}{D} \ll K_\perp^{eq}\,. \tag{11}$$

Using the typical value $q^\sigma = -0.1\ C/m^2$ for the surface charge density of the particle, we obtain $K^\sigma = \mu_e q^\sigma \approx 5 \times 10^{-9}$S and $K^{eq} = 2K^\sigma/L \approx 15$ S/m, an extremely large value compared to the typical bulk conductivity of our samples, $K_e \approx 3 \times 10^{-3}$ S/m. Roughly speaking, up to the relaxation frequency of the MWO effect ($\nu^{MWO} \gg \nu_c$), the beidellite particle behaves as a perfect conductor immersed in a good insulator. Neglecting small terms, we obtain for the MWO excess polarizability $\Delta A^{MWO} \approx -\frac{\varepsilon_0 V^p}{kT}\frac{4D}{\pi L}\varepsilon_e = -1.6 \times 10^{-9}$ $\mathrm{m^2V^{-2}}$, quite close to the experimental value -2.5×10^{-9} $\mathrm{m^2V^{-2}}$ for dilute solutions. This is exactly the result expected for *metallic* particles with the same L/D ratio, dispersed in a *perfect insulator* with dielectric constant ε_e.

4 Conclusions

We propose an electric-field experimental set-up optimized for the study of aqueous suspensions of colloidal particles. The traditional Kerr cell is replaced by a thin flat sample, sealed in an optical capillary, with a.c. electric field applied along the capillary axis by two external electrodes. This experimental geometry prevents the electrochemical degradation of the sample, minimizes heating and convection artifacts, and enables the direct microscopic observation of the textures throughout the experiment.

In this original cell geometry, we study the electric-field effects in the nematic and isotropic phases of aqueous suspensions of exfoliated natural beidellite clay particles with high aspect ratio, $D/L \approx 300$. In the nematic phase, our electric birefringence and SAXS experiments demonstrate very effective field-induced alignment, resulting in large "monodomais" with nematic director orientation perpendicular to the field and azimuthally degenerated. In isotropic samples, we observed a strong field-induced birefringence $\Delta n(E)$, saturating at moderate fields to a plateau Δn^{sat} proportional to the volume fraction ϕ. The field-induced order parameter $S(E)$ is negative and saturates to $S^{sat} = -0.5$, indicating a perfect "anti-nematic" order of the particles, *i.e.* the disk normals are perpendicular to the field, without preferred azimuthal direction. We show that the observed large anisotropy of excess polarizability ΔA is due to the strong induced polarization of the counterion cloud around the charged particle. The estimated equivalent conductivity of the beidellite particle $K^{eq} = 2K^\sigma/L$ is

several orders of magnitude larger than the bulk conductivity of the electrolyte K_e, resulting in a metal-like behavior of the beidellite disks under field.

Acknowledgements

Authors gratefully acknowledge the financial support from the ANR (Agence Nationale de la Recherche, “programme blanc” ANISO).

References

[1] L. Onsager (1949) *Ann. N.Y. Acad. Sci.* **51** 627.
[2] I.J. Langmuir (1938) *Chem. Phys.* 6 873.
[3] L.J. Michot *et al*. (2006) *Proc. Nat. Acad. Sci. USA* **103** 16101.
[4] L.J. Michot *et al*. (2008) *Langmuir* **24** 3127.
[5] E. Paineau *et al*. (2009) *J. Phys. Chem. B* **113** 15858.
[6] J.C.P. Gabriel, P. Davidson (2000) *Adv. Mat.* **12** 9.
[7] P. Davidson, J.C.P. Gabriel (2005) *Curr. Opin. Colloid Interface Sci*. 9 377.
[8] J. Kerr (1875) *Philosophical Magazine Series IV* **50** 337
[9] C.T. O’Konski, B.H. Zimm (1950) *Science* **111** 113.
[10] S.P. Stoylov, M.V. Stoimenova (2007) *Molecular and Colloidal Electro-Optics*, CRC/Taylor & Francis, Boca Raton.
[11] E. Fredericq, C. Houssier (1973) *Electric Dichroism and Electric Birefringence*, Clarendon Press, Oxford.
[12] E.D. Baily, B.R. Jennings (1973) *J. Colloid Interface Sci.* **45** 177.
[13] B.R. Jennings, B.L. Brown, H. Plummer (1970) *J. Colloid Interface Sci.* **32** 606.
[14] C.T. O’Konski, A.J. Haltner (1956) *J. Am. Chem. Soc.* **78** 3604.
[15] N. C. Stellwagen (1991) *Biopolymers* **31** 1651.
[16] I. Dozov *et al*. (2011) *J. Phys. Chem. B* **115** 7751.
[17] I. Lelidis, M. Nobili, G. Durand (1993) *Phys. Rev. E* **48** 3818.
[18] S. Forget, I. Dozov, P. Martinot-Lagarde (1999) *Mol. Cryst. Liq. Cryst. Sci. Technol. Sect. A-Mol. Cryst. Liq. Cryst.* **329** 1217.
[19] I. Dozov *et al*. (2000) *Appl. Phys. Lett.* **77** 4124.
[20] S. Lamarque-Forget, P. Martinot-Lagarde, I. Dozov (2001) *Jpn. J. Appl. Phys. Part 2 - Lett.* **40** L349.
[21] S. Lamarque-Forget *et al*. (2000) *Adv. Mater.* **12** 1267.
[22] P.-G. De Gennes, J. Prost (1993) *The Physics of Liquid Crystals*, 2nd ed., Clarendon Press, Oxford.
[23] A. F. Demirörs *et al*. (2010) *Langmuir* **26** 14466.
[24] K. Kang, J.K.G. Dhont (2010) *Soft Matter* **6** 273.
[25] B.J. Lemaire *et al*. (2005) *Faraday Discuss.* **128** 271.
[26] M. Imperor-Clerc, P. Davidson (1999) *Eur. Phys. J. B* **9** 93.
[27] W. Maier, A. Saupe (1959) *Zeitschrift Fur Naturforschung Part a-Astrophysik Physik Und Physikalische Chemie* **14** 882.

[28] Y. Meheust, K.D. Knudsen, J. O. Fossum (2006) *J. Appl. Cryst.* **39** 661.

[29] P. Martinot-Lagarde, H. Dreyfus-Lambez, I. Dozov (2003) *Phys. Rev. E* **67** 051710.

[30] J.B. Fournier, P. Galatola (2005) *Europhys. Lett.* **72** 403.

[31] W. Maier, A. Saupe (1958) *Zeitschrift Fur Naturforschung Part a-Astrophysik Physik Und Physikalische Chemie* **13** 564.

[32] A. Peterlin, H. A. Stuart (1939) *Zeitschrift Fur Physik* **11**2 129.

[33] L.D. Landau, E.M. Lifshitz (1960) *Electrodynamics of Continuous Media*, Pergamon Press, Oxford, New York.

[34] J.C. Maxwell (1954) *A Treatise on Electricity and Magnetism*, Unabridged 3d ed., Dover Publications, New York.

[35] K.W. Wagner (1914) *Arch. Elecktro. Technol.* **2** 371.

[36] C.T. O'Konski, A.J. Haltner (1957) *J. Am. Chem. Soc.* **79** 5634.

[37] C.T. O'Konski (1960) *J. Phys. Chem.* **64** 605.

[38] H.P. Schwan, G. Schwarz, J. Maczuk, H. Pauly (1962) *J. Phys. Chem.* **66** 2626.